In vivo characterization of a new abdominal aortic aneurysm mouse model with conventional and molecular MRI

Ahmed Klink[1], **Joeri Heynens**[2], **Beatriz Herranz, PhD**[1,3], **Mark E. Lobatto, MD**[1,4], **Teresa Arias, PhD**[1,3], **Honorius M. H. F. Sanders, PhD**[2], **Gustav J. Strijkers, PhD**[2], **Maarten Merkx, PhD**[2], **Klaas Nicolay, PhD**[2], **Valentin Fuster, MD, PhD**[3,5], **Alain Tedgui, PhD**[6], **Ziad Mallat, MD, PhD**[7], **Willem J.M. Mulder, PhD**[1], and **Zahi A. Fayad, PhD**[1,5,*]

[1]Translational and Molecular Imaging Institute, Mount Sinai School of Medicine, One Gustave L. Levy Place, 10029 New York, NY, USA. [2]Eindhoven University of Technology, Department of Biomedical Engineering, Laboratory of Chemical Biology, Eindhoven, The Netherlands. [3]Department of Epidemiology, Atherothrombosis and Imaging, Centro Nacional de Investigaciones Cardiovasculares (CNIC), Madrid, Spain. [4]Amsterdam Medical Center, Department of Vascular Medicine, Amsterdam, The Netherlands. [5]The Zena and Michael A. Wiener Cardiovascular Institute and the Marie-Josee and Henry R. Kravis Center for Cardiovascular Health, Mount Sinai Medical Center, New York, NY, 10029, USA. [6]Paris Cardiovascular Research Center, U970, Georges Pompidou European Hospital, Paris, France. [7]University of Cambridge, Department of Medicine, Cambridge, United Kingdom.

Abstract

Objectives—To use non-invasive conventional and molecular magnetic resonance imaging (MRI) to detect and characterize abdominal aortic aneurysms (AAAs) in vivo.

Background—Collagen is an essential constituent of aneurysms. Non-invasive MRI of collagen may represent an opportunity to help detect and better characterize AAA and initiate intervention.

Methods—We used an AAA C57BL/6 mouse model where a combination of angiotensin-II infusion and TGF-β neutralization results in AAA formation with incidence of aortic rupture. High-resolution multi-sequence MRI was performed to characterize the temporal progression of AAA. To allow molecular MRI of collagen, paramagnetic/fluorescent micellar nanoparticles functionalized with a collagen-binding protein (CNA-35) were intravenously administered. In vivo imaging results were corroborated with immunohistochemistry and confocal fluorescence microscopy.

*ADDRESS CORRESPONDENCE TO: Zahi A. Fayad, PhD, Atran Berg Laboratory Building Floor 8, Room AB8-826, 1428 Madison Avenue New York, NY 10029. Tel: 212-241-6858. Fax: 646-537-9693. zahi.fayad@mssm.edu.

Publisher's Disclaimer: This is a PDF file of an unedited manuscript that has been accepted for publication. As a service to our customers we are providing this early version of the manuscript. The manuscript will undergo copyediting, typesetting, and review of the resulting proof before it is published in its final citable form. Please note that during the production process errors may be discovered which could affect the content, and all legal disclaimers that apply to the journal pertain.

Disclosures
None.

Results—High-resolution multi-sequence MRI allowed the visualization of the primary fibrotic response in the aortic wall. As the aneurysm progressed, the formation of a secondary channel or dissection was detected. Further analysis revealed a dramatic increase of the aortic diameter. Injection of CNA-35 micelles resulted in a significant higher MR signal enhancement in the aneurysmal wall compared to non-specific micelles. Histological studies demonstrated the presence of collagen in regions of MR signal enhancement and confocal microscopy proved the precise colocalization of CNA-35 micelles with collagen-I. In addition, in a proof of concept experiment, we have shown the potential of CNA-35 micelles to discriminate between stable AAA lesions and aneurysms that were likely to rapidly progress/rupture.

Conclusion—Multi-sequence MRI allowed longitudinal monitoring of AAA progression while the presence of collagen was visualized by nanoparticle-enhanced MRI.

Keywords

MRI; molecular imaging; abdominal aortic aneurysm; collagen

Introduction

Abdominal aortic aneurysms are permanent dilatations of the abdominal aorta exceeding the normal diameter by more than 50% and present a life-threatening degenerative disease. They occur in 5-9% of the population over the age of 65 and are the 10th leading cause of death in the Western Countries[1]. AAA progression is characterized by a long period of asymptomatic growth of the abdominal aorta. Once it reaches 5.5 cm it has an increased chance of rupture with a mortality of over 80%. Surgery and EVAR are currently the only interventions for patients diagnosed with AAA. This is costly and associated with a high morbidity and mortality rate. Generally, surgery or EVAR are recommended when the AAA reaches a size of 55 mm or if the expansion rate is greater than 1 cm/year[2]. Although currently the best predictor of aneurysm expansion is the baseline size at diagnosis[3], the prognosis remains complex due to the nonlinearity and unpredictability of expansion rates[4]. More specific prognostic predictors would offer the chance to better select intervention strategies for individual patients. Different animal models have been developed in the past several years to improve the understanding of AAA pathophysiology. Recently, Wang and colleagues[5] introduced a model where a combination of Ang-II and anti-TGF-β administered to C57BL/6 wild type mice leads to AAA formation and occurrence of fatal AAA rupture as high as 80%. Currently, this is the only animal model that displays such a relevant rate of AAA rupture, thereby enabling monitoring of the mechanisms at play in this fatal process.

The degradation of the extracellular matrix (ECM) in the medial wall is key in the formation, progression and rupture of AAA[6]. Particularly, the turnover of collagen, an essential component of the ECM, is known to be responsible for the remodeling that occurs in the adventitia. Recent studies indicate that perturbations in collagen micro-architecture and networks, probably as a result of collagen degradation and inappropriate collagen deposition, may alter vessel wall response to mechanical load and lead to vessel wall failure [7]. Therefore, imaging collagen in AAA might provide valuable information about the state of aneurysm development and the identification of AAAs prone to severely progress or rupture.

In the current work, we first explored the use of multi-sequence high-field MRI to characterize the development of AAA in the aforementioned model. Then, we applied recently developed fluorescent/paramagnetic nanoparticles[8], functionalized with a collagen-specific protein (CNA-35)[9-13] to identify presence of collagen in the aneurysmal wall with molecular MRI. Finally, in a proof-of-concept experiment, we studied the potential of CNA-35 micelles to discriminate between stable AAAs and aneurysms prone to progress and eventually rupture.

Methods

Animal Model

All the procedures were approved by the Mount Sinai School of Medicine animal care committee (Institutional Animal Care and Use Committee). C57BL/6J male mice (Jackson Laboratories, Bar Harbor, Maine) between the ages of 8 to 12 weeks were used. As described in more detail by Wang et al.[5], AAAs were induced in wild type mice by continuous infusion of Ang-II at 1000 ng/kg/min for a maximum of 28 days, along with systemic neutralization of TGF-β. Briefly, animals were anesthetized with isoflurane (4% induction, 1.5% maintenance) and mini-pumps (Alzet, model 2004) that contained 200 μl of Ang-II were implanted subcutaneously. To achieve systemic neutralization of TGF-β, intra-peritoneal injections of an anti-TGF-β antibody (dose: 20 mg/kg) were performed every other day, which results in AAAs formation in the suprarenal region of the aorta.

Multi-sequence in vivo MR imaging of AAA progression

AAAs were induced in a group of mice as described above (n=3). MRI scanning was performed on a 9.4T small animal vertical bore MRI scanner (Bruker BioSpec, Bruker, Germany). Each animal was placed in the center of a whole-body coil (35 mm inner diameter), under continuous isoflurane anesthesia, which was positioned in the scanner. The animals were connected to a respiratory-rate monitor and the flow of anesthetic gas was constantly regulated to maintain a breathing rate of 60 breaths per minute. Baseline MRI scanning was followed by scans every other day until sacrifice. Each scan session started with a pilot scan with 3 orthogonal slices, followed by high resolution black blood T1W, T2W and PDW spin echo imaging of which the exact parameters are reported in the Supplementary Material. The suprarenal region of the aorta encompassing 22 mm immediately superior to the right renal artery was imaged. Subsequently, a TOF angiography sequence was used to visualize the blood flow and generate a three dimensional reconstruction of the aorta to allow the visualization of vessel dilation.

Molecular MR imaging of collagen

AAAs were induced in wild type mice (n=10) according to the protocol described above. The presence of an aneurysm was assessed with MR angiography. CNA-35 micelles or the mutant Y175K CNA-35 micelles[12] (dose 50 μmol Gd/kg) were injected in the tail vein of the animals (n=5 for each group). The mice were imaged pre and 32 hours post injection to allow proper clearance of the micelles from the circulating blood, using a T1W spin echo sequence – with the same parameters as used for the multi-spectral imaging group (Supplementary Material). To insure that AAA remodeling remained minimal between pre

and post imaging sessions, the injections of anti-TGF-β antibody were terminated prior to the imaging sessions. Animals that received subcutaneous infusion and intra-peritoneal injections of saline were injected with CNA-35 micelles and used as controls (n=4). In addition, the half-life of CNA-35 micelles was investigated by collecting blood samples at different time points over a period of 24 hours. The blood samples were imaged on the IVIS optical system and photon counts were measured to determine the half-life.

Predictive value of (molecular) MRI for the assessment of experimental AAA

AAA were induced in C57BL/6 mice (n=8) as described above (10mg/kg). To study whether CNA-35 micelles enhanced molecular MRI can discriminate between stable AAA lesions and aneurysms that are prone to severely progress or rupture, animals were MR imaged after i.v. administration of CNA-35 micelles at day 5 and day 15 after the onset of AAA. These animals were monitored for death or survival, while aneurysm severity (stage I to stage IV) was assessed by looking at aneurysm morphology as previously described[14]. Mice that suffered from ruptured aneurysms were classified as Stage IV.

Image analysis and statistics

Pre and post MR images were analyzed using OsiriX DICOM Viewer (Geneva, Switzerland). Each slice was co-registered using the spinal cord as a landmark. AAAs were identified on the pre injection images. An ROI was drawn around the aneurysmal wall and the average signal intensity was measured (I_{wall}) over 10 slices throughout the aneurysm. In addition, ROIs were also drawn in the surrounding muscle as well as in the noise, and the average signal intensity and standard deviation of the noise were measured respectively (I_{muscle}, σ_{noise}). SNRs were calculated for the wall and the muscle

$\left(SNR_{Wall} = \frac{I_{wall}}{\sigma_{Noise}}, SNR_{Muscle} = \frac{I_{Muscle}}{\sigma_{Noise}} \right)$. The contrast to noise ratio was calculated

$\left(CNR_{WM} = \frac{SNR_{Wall}}{SNR_{Muscle}} \right)$ and further normalized to the pre-injection values

$\left(CNR_{Norm} = \frac{CNR_{WMpost}}{CNR_{WMpre}} \right)$. Finally, the normalized percentage signal enhancement (%NSE) was determined ($\%NSE = (CNR_{Norm} - 1) \# 100$). The data are presented as mean ± S.D. A one-way and two-way ANOVA test were performed to determine statistical significance. A post-hoc Tukey test was performed to compare each of the three groups injected with CNA-35 micelles or mutant CNA-35 micelles. A Bonferroni post-hoc test was performed to compare the %NSE of stage II, III and IV aneurysms at day 5 and day 15 of AAA development. A p value under 0.05 was considered statistically significant. Statistical analysis was performed using PRISM (Graphpad Software, La Jolla, CA).

Immunohistochemistry and confocal microscopy

Animals were sacrificed by an isoflurane overdose. Transcardiac perfusions through the left ventricle were carried out with saline and paraformaldehyde (4%). The suprarenal aorta was excised, collected in OCT and frozen for further histology examination. CME staining was performed to stain for collagen and elastin fibers. In addition, type I collagen and macrophage CD68 staining was performed using a primary rabbit anti-mouse type I collagen antibody and a primary rat anti-mouse CD68 antibody respectively (Santa Cruz

Biotechnology, Delaware); the primary antibodies were detected using appropriate secondary antibodies coupled to an Alexa-647 fluorophore. For each animal, 10 representative sections were chosen, fixed in 4% paraformaldehyde and washed twice in PBS. The sections were blocked with 2% goat serum in PBS for 20 minutes at room temperature. After blocking, the sections were incubated with the collagen-I primary antibody or CD68 primary antibody (1:100 dilution) for an hour. After washing with PBS, the secondary antibody was added for 30 minutes. Finally, the autofluorescence of the tissue was reduced using copper sulfate and sections were mounted with DAPI-containing Vecta Shield mounting medium (Vector, Burlingame, CA, USA) and sealed with coverslips, shielded from light, and kept at 4°C until CLSM was performed within 48 hours. Sections incubated with the secondary antibody only were used as negative controls. CLSM imaging was performed with a Leica Sp5DM microscope (Leica Microsystems, Wetzlar, Germany). Adjacent sections were stained for collagen-I and macrophages to study their respective localization with regard to the CNA-35 micelles labeled with rhodamine.

Results

Characterization and in vitro binding experiments

The synthesis and a schematic of the paramagnetic micelles are included in the Supplementary Material. The size of the micelles before conjugation was 14 ± 1.5 nm whereas the CNA-35 and mutant CNA-35 coupled micelles had a mean size of 25 ± 3 nm. Phosphate determination and protein determination yielded a lipid:protein ratio of approximately 50:1 corresponding to approximately 2 proteins per micelle. The ionic relaxivity, a measure of MRI contrast generating potency[15], of bare, CNA-35 or mutant CNA-35 conjugated micelles was 12 mM^{-1}s^{-1}. CNA-35 is a natural collagen binding protein that has been shown to have affinity for collagen fibers. Indeed, collagen fibers contain a high density of binding sites with both high and low affinity for the CNA-35 protein resulting in an average constant dissociation value K_d of 500 nM[11]. Our in vitro binding experiment (described in the Supplementary Material) corroborated these previously published findings[11]. We observed an apparent binding of the CNA-35 micelles to collagen after extensive washing, while little binding occurred for mutant CNA-35 or unconjugated micelles (Supplementary Material figure 1B). A second in vitro experiment was performed to further confirm these findings and to investigate the collagen binding of Cy5.5 labeled CNA-35 micelles with NIRF imaging using the IVIS optical imaging system. Similar to the plate reader studies we found a clear binding of the CNA-35 micelles to collagen (Supplementary Material figure 1C). Finally, the blood circulation half-life of the CNA-35 micelles in male C57BL/6 mice (n=2) was determined to be 4.3 hours.

Multi-sequence in vivo imaging of AAA progression

AAAs were induced in male C57BL/6 mice via continuous infusion of Ang-II and administration of anti-TGF-ß every other day. The abdominal region of these mice was imaged using high-resolution multi-sequence MRI to monitor the temporal progression of AAA at the anatomical level. T1W, T2W and PDW MRI as well as MRI angiography were performed. Multi-sequence MRI allowed the visualization of the primary fibrotic response in the aortic wall at day 3. It also showed luminal stenosis and medial rupture with blood

infiltrating the adventitial tissue at 6 days after AAA induction (figure 1A, B and C). At day 8, the adventitia appeared to be extensively destructed with the formation of a double channel clearly visible on different sequences (figure 1A. B and C). The three dimensional reconstruction resulting from the time of flight angiography confirmed the aortic dilatation and the presence of blood infiltrating the adventitial tissue (figure 1D, arrow). Further analysis showed a dramatic increase in the diameter of the aorta, reaching 50% growth at day 5 and up to a 150% growth on day 15 (figure 1F). To corroborate the in vivo findings, immunohistological examination of the aortas was performed upon the animals' death. The results confirmed the presence of AAA and allowed the precise validation of several features of vessel wall remodeling observed by in vivo MRI. An extreme degradation of the ECM was observed due to massive destruction of adventitial collagen. Only a thin cap remained visible on the outer edge of the aneurysmal wall preventing the vessel from rupturing. Intense degradation of the elastin fibers as well as the complete rupture of the medial layer of the aorta was clearly identified (figure 1E, arrow). Due to the rupture blood originating from the aortic lumen was able to infiltrate the adventitia, thereby forming a secondary lumen referred to as false channel or dissection (figure 1E). The resulting increase of the aortic diameter was visibly noted.

In vivo molecular imaging of collagen

Although high-resolution multi-sequence MRI allows the characterization of AAA progression on an anatomical level, it does not provide any information on the underlying molecular biological processes. Therefore, we decided to evaluate the presence of collagen in the same mouse model as it represents a key constituent of aneurysms. To that end, collagen specific CNA-35 micelles were synthesized and injected for nanoparticle-enhanced MR imaging. Prior to the injection of micelles, the presence of aneurysms was evaluated using MR angiography. T1W MR images were then acquired before and 32 hours after injection of CNA-35 or mutant CNA-35 micelles. In mice injected with CNA-35 micelles a clear signal enhancement in the aneurysmal region was observed (figure 2A), while a significantly lower signal enhancement was visible after the injection of mutant CNA-35 micelles. As shown in figure 2B, data analysis of the MR images revealed an 80.15 ± 37 percent increase in NSE after injection of CNA-35 micelles compared to a 30.90 ± 19 percent increase after the injection of mutant CNA-35 micelles (n=5, p=0.0048 – one way ANOVA test, p<0.05 – post-hoc Tukey test). No enhancement was observed in healthy animals injected with CNA-35 micelles.

Examination of the corresponding histological slices stained with CME showed an advanced degree of adventitial destruction with the presence of collagen in the areas of MR signal enhancement (figure 3B, C, F, G). Importantly, further examination by confocal microscopy demonstrated the colocalization of the CNA-35 micelles (red) with collagen-I (green) in the adventitia (figure 3D). In animals injected with mutant CNA-35 micelles, the fluorescent signal originating from the micelles was found to be nearly nonexistent in the regions that stained positively for collagen-I (figure 3H). In addition, CLSM images of macrophage stained with a CD68 antibody, showed no association between macrophages and CNA-35 or mutant CNA-35 micelles (data not shown). It is noteworthy that mutant CNA-35 micelles were not associated with any specific biological structures. In addition, the collagen MR

signal enhancement pattern observed in different animals allowed differentiation between collagen-rich and collagen poor lesions as observed on corresponding CME stains (figure 4).

Ex vivo fluorescence imaging

To corroborate the CNA-35 micelles enhanced in vivo MRI results and to investigate their spatial distribution in the aorta, Cy5.5-labeled micelles were injected in mice after AAA development as well as in healthy animals. NIRF imaging, a so-called hotspot imaging technique[16], allows the visualization of the Cy5.5 labeled micelles with high sensitivity in intact aortas[17,18]. Mice were sacrificed 32 hours post injection and the excised aortas were imaged with NIRF imaging. Cy5.5 labeled CNA-35 micelles were clearly observed in the AAA region (Supplementary Material, figure 2). In comparison, healthy animals and non-injected AAA animals marginally displayed fluorescent signal, further supporting the specific binding of CNA-35 micelles in the aneurysmal region.

Predictive value of (molecular) MRI for the assessment of experimental AAA

As described above, the injection of CNA-35 micelles allowed the discrimination between collagen-poor and collagen-rich lesions (figure 4). It has been shown in the literature that low levels of collagen were associated with AAA progression and ultimately rupture[7]. Hence, we hypothesized that CNA-35 micelles had the potential to discriminate between stable AAA lesions and aneurysms that are prone to progress or rupture. We imaged CNA-35 injected animals at day 5 and day 15 of AAA development and subsequently monitored them for survival. Upon death or sacrifice, the aneurysm severity was evaluated by looking at the aneurysm morphology as previously described[14]. Administration of anti-TGF-β in Ang-II infused mice led to mortality from aneurysm rupture (stage IV) in 3 mice while the remaining 5 animals survived bearing stage II and III AAA. All the main features of human aneurysms ranging from the fibrotic response around the vessel wall to signs of medial dissection and formation of a secondary channel were observed.

As shown in figure 5, animals that were morphologically classified with stage II aneurysms showed marked enhancement after CNA-35 administration at day 5 and day 15 of aneurysmal development, suggesting a collagen rich response of the aortic wall. These lesions demonstrated to be stable as no aortic dissection and medial rupture were observed, and the animal survived the 28 day period of Ang-II + anti-TGF-β administration. In contrast, all the mice retrospectively classified with stage III and stage IV aneurysms (n=5) exhibited a dissection of the media at day 5 (figure 5A, arrow) and showed a marked decrease of approximately 30% in NSE in both groups relative to stage II AAAs (48.50 ± 4.950 vs. 72.01 ± 10.47, $p > 0.05$ and 46.68 ± 7.652 vs. 72.01 ± 10.47, $p > 0.05$ respectively) (figure 5B). Imaging at day 15 showed a critical progression of AAA development with an extensive remodeling of the vessel wall and presence of a secondary channel. Ruptured stage IV aneurysms showed little signal enhancement after CNA-35 injection, suggesting a lower collagen content as opposed to non-ruptured stage II and III aneurysms (52.13 ± 8.408 vs. 120.7 ± 19.49, $p < 0.001$ and 52.13 ± 8.408 vs. 87.51 ± 3.521, $p < 0.05$ respectively) (figure 5B). Consistent with this hypothesis, histological examination upon death of the animals at day 19, 22 and 23, showed substantial collagen degradation in fatal aneurysms as compared to viable stage II and stage III AAAs. A two-way ANOVA test

showed that both factors (stage of aneurysm and time) significantly alter %NSE (p=0.0027 and p=0.0024 respectively) and that there is a significant interaction between the two factors (p=0.0407). These findings show a potential for CNA-35 micelles to discriminate between stable AAA lesions with important collagen content and aneurysms that are likely to rapidly progress and eventually rupture.

Discussion

In the present study, we demonstrated the ability of high-resolution conventional and molecular MRI to detect key anatomical features of aneurysmal progression and to identify the presence of collagen in the aneurysmal wall in a new AAA mouse model. Conventional multi-sequence black blood MRI permitted the visualization of the different stages of AAA progression. Over the course of aneurysm development we demonstrated the accurate identification of the primary fibrotic response in the vessel wall with consequent luminal stenosis. As the aneurysm progressed we visualized the medial rupture with blood infiltrating the remodeled adventitia, which resulted in the formation of a double channel. The ensuing increase in aortic diameter was clearly noted and quantified. Histological examination upon the death of the animals matched the MR observations and confirmed the presence of the aforementioned landmarks of aneurysmal progression.

Molecular MRI, upon the intravenous administration of collagen targeted CNA-35 micelles, provided valuable information about the presence of collagen in the aneurysmal wall. The injection of CNA-35 micelles resulted in a significantly higher MR signal enhancement than the injection of mutant CNA-35 micelles. Histological staining for collagen in corresponding sections confirmed the presence of collagen in the areas of MR signal enhancement. Further examination with fluorescent confocal microscopy demonstrated the precise colocalization of CNA-35 micelles with collagen stained in the remodeled adventitia. Importantly, in a proof-of-concept experiment, CNA-35 micelle enhanced MRI allowed the differentiation between stable AAA lesions and aneurysms that are likely to rapidly progress and rupture.

Imaging technologies in general, and ultrasound imaging and CT in particular, are currently used to obtain information related to AAA in humans[19,20]. A CT angiography is routinely performed to obtain pre-operative anatomical information on the aneurysm and its relationship to surrounding structures[21]. However, disadvantages include the use of contrast and exposure to radiation. As for ultrasound imaging, it is widely used to monitor AAA progression but it provides little contrast and suffers from a poor signal to noise ratio, which limits the ability to obtain a detailed evaluation of the remodeled adventitia, particularly in pre-clinical studies involving small animal models. Although some recent reports have shown the ability of ultrasound Doppler to identify medial rupture and differentiate between the lumen and the false channel in mice[5], the resolution of ultrasound remains subpar as compared to MRI. Recently, MRI has been used successfully by Turner et al.[22] to assess the development of an Ang-II induced aneurysm model in hypercholesterolemic mice. The authors showed that MR measurements of AAA area performed on a bright blood sequence precisely correlated with the AAA area measured by histology. In the present study, the aortic diameter measured with three different MR methods (T1W, T2W and PDW) was

evaluated at each imaging time point. The results showed a fast increase of the aortic diameter reaching 50 %, the minimum value to define an aneurysm, 5 days after the initiation of the experiment on average. In addition to providing aortic diameter measurements, multi-sequence black-blood imaging offers superior contrast compared to bright-blood sequences for the examination of vessel wall remodeling during AAA formation and progression. Furthermore, and similarly to bright-blood imaging, it allowed the accurate identification of the medial rupture and formation of a double channel. Particularly, on the T1W sequence, the medial rupture was clearly identifiable as soon as three days after AAA induction compared to the T2W and PDW sequences that did not allow such evident visualization until 6 days after aneurysm initiation (figure 1B). In addition, multi-sequence black blood imaging also offered adequate resolution to image the medial-adventitial interface. Indeed, despite various degrees of aortic stenosis caused by different degrees of collagen degradation and thrombus formation, the lumen always remained easily distinguishable from the remodeled adventitia, even upon blood extravasation in the adventitial space. Multi-sequence black-blood MR imaging offers the benefit of an increased accuracy in characterizing the anatomical features of AAA temporal progression.

One of the biological processes underlying AAA formation and progression is the degradation of the extracellular matrix, in particular collagen. Members of the MMP and cysteine protease families can degrade the highly protease-resistant structures of type I and type III collagen[23-25]. After the destabilization of the collagen structure, other less specific proteases can further degrade collagen. This increased collagen degradation in combination with inadequate collagen deposition has been associated with the progression and ultimately rupture of AAAs. Therefore, imaging collagen might offer additional insights about the state of aneurysm progression. CNA-35 consists of two N-domains (N1, N2) from a collagen adhesion protein originating from *Staphylococcus aureus* and was used as a targeting ligand. Its specificity for collagen was previously demonstrated in vitro and in vivo[9,10,12,13]. In its open conformation, the CNA-35 protein can fold and lock around the collagen fiber[11]. This binding process implies that CNA-35 micelles would also adhere to individual triple helical fibers of collagen, which are hardly present in healthy tissue, in addition to binding to mature collagen fibers. Degraded collagen and newly formed collagen fibers, highly present in advanced stages of AAA are associated with high portions of free triple helices. Therefore, the bright signal enhancement observed in the aneurysmal wall of animals injected with CNA-35 micelles might derive from a combination of the micelles' increased affinity to mature collagen fibers as well as to unstructured collagen present in AAA[7]. When CNA-35 micelles were injected in animals in healthy animals, no MR signal enhancement was observed (figure 2B). Given the size of these particles (25nm), their inability to penetrate healthy tissue is likely to be the limiting factor to collagen binding. It is apparent that the degree of adventitial collagen degradation relates to the stage of aneurysmal severity. In fact, it has been shown previously that increased collagen degradation is associated with AAA progression and ultimately rupture[7]. Thus, one could argue that increased level of collagen in the aortic wall stabilizes the aneurysm. We therefore hypothesized that CNA-35 micelles would allow the distinction between stable collagen-rich AAA lesions and collagen poor lesions that are more likely to progress and rupture. To that

end, we designed a proof-of-concept experiment where the normalized signal enhancement relative to CNA-35 injection was calculated at early and late stage of AAA development and correlated with the aneurysm severity determined by their morphology (stage I to stage IV). Our findings showed the ability of CNA-35 micelles to identify stable aneurysms as the collagen-rich response of the aortic wall of non-complicated lesions was recognizable with a high NSE percentage value (figure 5). In addition, a decrease of CNA-35 uptake at early stage of aneurysmal development (day 5) in stage III and IV aneurysms was associated with a rupture of the medial layer of the aorta and subsequent critical AAA progression. Interestingly, the medial rupture seemed to occur in the areas of lowest CNA-35 uptake (figure 5, arrow). Importantly, lesions with the lowest NSE percentage value that did not increase at follow-up were identified as fatal stage IV aneurysms and presented critical collagen degradation as compared to viable stage III aneurysms.

Although collagen is likely not the only biological component at play in AAA progression and rupture, its precise monitoring may benefit diagnosis and staging of the aneurysm. Our results show that CNA-35 micelles enhanced MRI represents an extremely interesting concept for the detection of collagen in the aneurysmal wall and has potential for predicting the course of AAA development. However, due to the low number of animals per group in that experiment, more extensive studies are necessary to confirm the predictive value of CNA-35 micelle enhanced MRI in assessing AAA progression/rupture.

The current clinical guidelines[26] for the management of aneurysms are mainly based on the size of aneurysms and recommend repeated anatomical imaging every 3 to 6 months for aneurysms greater than 4 cm. Endovascular repair or surgery is recommended for AAAs that are greater than 5.5 cm, symptomatic or fast growing. Intervention is not indicated when these criteria are not met as the chance of rupture is under 2.1%[25]. The high rate of mortality associated with reparative surgery would expose patients to unnecessary risks. Non-invasive imaging approaches, such as high-resolution multi-sequence black blood MRI and collagen targeted MRI described in this study, could ultimately improve the identification of patients at risk and facilitate the clinical management of abdominal aortic aneurysms[27]. It is noteworthy that other biological targets involved in AAA pathology are also persuaded as imaging targets in an effort to improve the characterization of the aneurysmal wall. Nahrendorf et al. developed a macrophage-targeted nanoparticle for PET-CT detection of inflammation in aortic aneurysms[28]. Recently, a pilot study used ultrasmall superparamagnetic iron oxide nanoparticles uptaken to predict aneurysm growth in humans[29]. In addition, such anatomical and biological information obtained may replace the pre-operative need of a CT angiography.

In conclusion, we demonstrated that high-resolution multi-sequence MRI allowed the visualization of critical features of vessel remodeling inherent to AAA formation and progression, while collagen-targeted nanoparticle-enhanced MRI permitted the non-invasive detection of collagen, an essential component in aneurysm pathology.

Supplementary Material

Refer to Web version on PubMed Central for supplementary material.

Acknowledgments

Abbreviations list

AAA	Abdominal aortic aneurysm
EVAR	Endovascular Aortic Repair
Ang-II	Angiotensin-II
MRI	Magnetic resonance imaging
MR	Magnetic resonance
ECM	Extracellular matrix
T1W	T1-weighted
T2W	T2-weighted
PDW	Proton density-weighted
TOF	Time of flight
ROI	Region of interest
SNR	Signal to noise ratio
CNR	Contrast to noise ratio
CME	Combined Masson Elastin
CLSM	Confocal laser scanning microscopy
NIRF	Near infrared fluorescence

References

1. Thompson RW, Geraghty PJ, Lee JK. Abdominal aortic aneurysms: basic mechanisms and clinical implications. Curr Probl Surg. 2002; 39:110–230. [PubMed: 11884965]

2. Sakalihasan N, Limet R, Defawe OD. Abdominal aortic aneurysm. Lancet. 2005; 365:1577–1589. [PubMed: 15866312]

3. Michel JB. Contrasting outcomes of atheroma evolution: intimal accumulation versus medial destruction. Arterioscler Thromb Vasc Biol. 2001; 21:1389–192. [PubMed: 11557661]

4. Powell JT, Brady AR. Detection, management, and prospects for the medical treatment of small abdominal aortic aneurysms. Arterioscler Thromb Vasc Biol. 2004; 24:241–245. [PubMed: 14604835]

5. Wang Y, Ait-Oufella H, Herbin O, et al. TGF-beta activity protects against inflammatory aortic aneurysm progression and complications in angiotensin II-infused mice. J Clin Invest. 2010; 120:422–432. [PubMed: 20101093]

6. Hellenthal FA, Buurman WA, Wodzig WK, Schurink GW. Biomarkers of abdominal aortic aneurysm progression. Part 2: inflammation. Nat Rev Cardiol. 2009; 6:543–552. [PubMed: 19546866]

7. Abdul-Hussien H, Soekhoe RG, Weber E, et al. Collagen degradation in the abdominal aneurysm: a conspiracy of matrix metalloproteinase and cysteine collagenases. Am J Pathol. 2007; 170:809–817. [PubMed: 17322367]

8. Mulder WJ, Griffioen AW, Strijkers GJ, Cormode DP, Nicolay K, Fayad ZA. Magnetic and fluorescent nanoparticles for multimodality imaging. Nanomedicine (Lond). 2007; 2:307–324. [PubMed: 17716176]

9. Megens RT, Oude Egbrink MG, Cleutjens JP, et al. Imaging collagen in intact viable healthy and atherosclerotic arteries using fluorescently labeled CNA35 and two-photon laser scanning microscopy. Mol Imaging. 2007; 6:247–260. [PubMed: 17711780]

10. Boerboom RA, Krahn KN, Megens RT, van Zandvoort MA, Merkx M, Bouten CV. High resolution imaging of collagen organisation and synthesis using a versatile collagen specific probe. J Struct Biol. 2007; 159:392–399. [PubMed: 17572104]

11. Zong Y, Xu Y, Liang X, et al. A 'Collagen Hug' model for Staphylococcus aureus CNA binding to collagen. EMBO J. 2005; 24:4224–4236. [PubMed: 16362049]

12. Helms BA, Reulen SW, Nijhuis S, de Graaf-Heuvelmans PT, Merkx M, Meijer EW. High-affinity peptide-based collagen targeting using synthetic phage mimics: from phage display to dendrimer display. J Am Chem Soc. 2009; 131:11683–11685. [PubMed: 19642697]

13. Sanders HM, Strijkers GJ, Mulder WJ, et al. Morphology, binding behavior and MR-properties of paramagnetic collagen-binding liposomes. Contrast Media Mol Imaging. 2009; 4:81–88. [PubMed: 19191276]

14. Manning MW, Cassi LA, Huang J, et al. Abdominal aortic aneurysms: fresh insights from a novel animal model of the disease. Vasc Med. 2002; 7(1):45–54. [PubMed: 12083734]

15. Duguet E, Vasseur S, Mornet S, Devoisselle JM. Magnetic nanoparticles and their applications in medicine. Nanomedicine (Lond). 2006; 1:157–168. [PubMed: 17716105]

16. Bulte JW. Hot spot MRI emerges from the background. Nat Biotechnol. 2005; 23:945–946. [PubMed: 16082363]

17. Sosnovik DE, Nahrendorf M, Deliolanis N, et al. Fluorescence tomography and magnetic resonance imaging of myocardial macrophage infiltration in infarcted myocardium in vivo. Circulation. 2007; 115:1384–1391. [PubMed: 17339546]

18. Sosnovik DE, Schellenberger EA, Nahrendorf M, et al. Magnetic resonance imaging of cardiomyocyte apoptosis with a novel magneto-optical nanoparticle. Magn Reson Med. 2005; 54:718–724. [PubMed: 16086367]

19. Martin-McNulty B, Vincelette J, Vergona R, Sullivan ME, Wang YX. Noninvasive measurement of abdominal aortic aneurysms in intact mice by a high-frequency ultrasound imaging system. Ultrasound Med Biol. 2005; 31:745–749. [PubMed: 15936490]

20. Barisione C, Charnigo R, Howatt DA, Moorleghen JJ, Rateri DL, Daugherty A. Rapid dilation of the abdominal aorta during infusion of angiotensin II detected by noninvasive high-frequency ultrasonography. J Vasc Surg. 2006; 44:372–376. [PubMed: 16890871]

21. Willmann JK, Wildermuth S, Pfammatter T, et al. Aortoiliac and renal arteries: prospective intraindividual comparison of contrast-enhanced three-dimensional MR angiography and multi-detector row CT angiography. Radiology. 2003; 226:798–811. [PubMed: 12601190]

22. Turner GH, Olzinski AR, Bernard RE, et al. In Vivo Serial Assessment of Aortic Aneurysm Formation in Apolipoprotein E-Deficient Mice via MRI. Circulation: Cardiovascular Imaging. 2008; 1:220. [PubMed: 19808546]

23. Lindholt JS, Erlandsen EJ, Henneberg EW. Cystatin C deficiency is associated with the progression of small abdominal aortic aneurysms. Br J Surg. 2001; 88:1472–1475. [PubMed: 11683743]

24. Lutgens SP, Cleutjens KB, Daemen MJ, Heeneman S. Cathepsin cysteine proteases in cardiovascular disease. Faseb J. 2007; 21:3029–3041. [PubMed: 17522380]

25. Sakalihasan N, Delvenne P, Nusgens BV, Limet R, Lapiere CM. Activated forms of MMP2 and MMP9 in abdominal aortic aneurysms. J Vasc Surg. 1996; 24:127–133. [PubMed: 8691515]

26. Hirsch AT, Haskal ZJ, Hertzer NR, et al. ACC/AHA Guidelines for the Management of Patients with Peripheral Arterial Disease (lower extremity, renal, mesenteric, and abdominal aortic): a collaborative report from the American Associations for Vascular Surgery/Society for Vascular Surgery, Society for Cardiovascular Angiography and Interventions, Society for Vascular Medicine and Biology, Society of Interventional Radiology, and the ACC/AHA Task Force on Practice Guidelines (writing committee to develop guidelines for the management of patients with peripheral arterial disease)--summary of recommendations. J Vasc Interv Radiol. 2006; 17:1383–97. quiz 1398. [PubMed: 16990459]

27. Klink A, Hyafil F, Rudd J, et al. Diagnostic and therapeutic strategies for small abdominal aortic aneurysms. Nat Rev Cardiol. 2011; 8(6):338–47. [PubMed: 21304473]

28. Nahrendorf M, Keliher E, Marinelli B, et al. Detection of macrophages in aortic aneurysms by nanoparticle positron emission tomography-computed tomography. Arteriosclr Thromb Vasc Biol. 2011; 31(4):750–7.

29. Richards JM, Semple SI, Macgillivray TJ, et al. Abdominal aortic aneurysm growth predicted by uptake of ultrasmall superparamagnetic particles of iron oxide: a pilot study. Circ Cardiovasc Imaging. 2011; 4(3):274–81. [PubMed: 21304070]
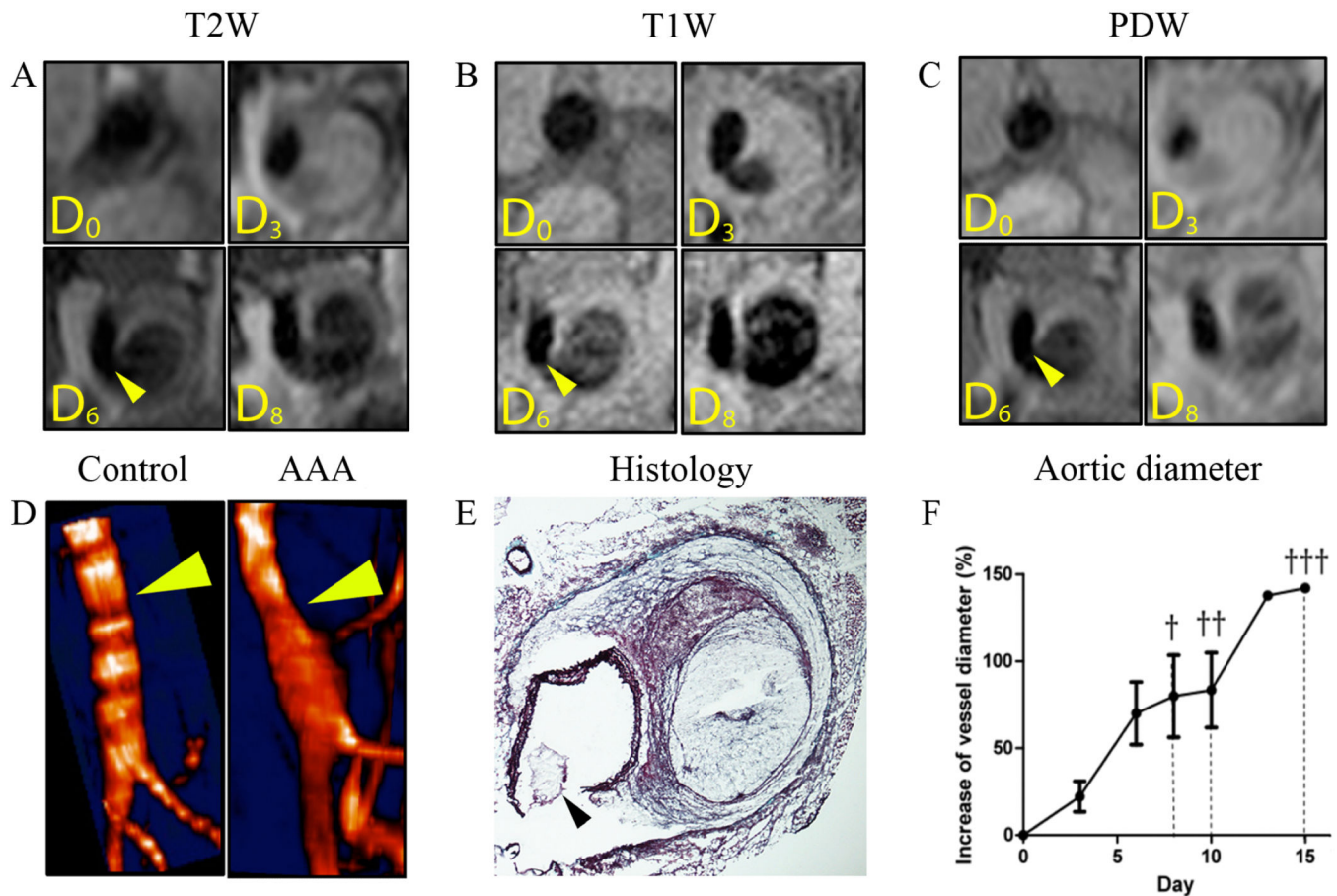
Figure 1. High-resolution multi-sequence MRI of AAA progression over the course of 8 days
(A) T2-weighted (T2W) black blood imaging of AAA progression over the course of 8 days. The primary fibrotic response and luminal stenosis is visualized at 3 days after AAA induction in the upper right corner. At 6 days, the medial rupture with blood infiltrating the adventitial tissue is visible (arrow). At day 8, the formation of a second channel is clearly visible in the bottom right corner. **(B)** T1-weighted (T1W) black blood imaging of AAA progression over the course of 8 days. Medial rupture is visible here as soon as 3 days after the induction of AAA in the upper right corner. The formation of a false channel with probably disturbed blood flow extravasating in the adventitia is visualized at day 6. At day 8, the formation of the false channel is clearly visible. **(C)** Proton Density-weighted (PDW) black blood imaging of AAA progression over the course of 8 days. The primary fibrotic response, the medial rupture and false channel formation were all observed respectively at day 3, day 6 and day 8 after AAA induction. **(D)** 3D MR Time of flight angiography of a healthy aorta and AAA. Aortic dilation due to medial rupture and blood infiltration in the adventitia is visible (arrow). **(E)** Histology with Combined-Masson Elastin (CME) staining confirmed the presence of the medial rupture and degradation of the elastic lamina as well as the extreme remodeling of the adventitia and formation of a false channel. **(F)** The increase of aortic diameter was averaged from the 3 sequences (T1W, T2W, PDW) at each imaging time point and plotted. A 50% increase, which is the minimum size to define the presence of

AAA was reached 5 days after AAA induction. The days of animals' death from AAA rupture were noted and are marked with a cross.
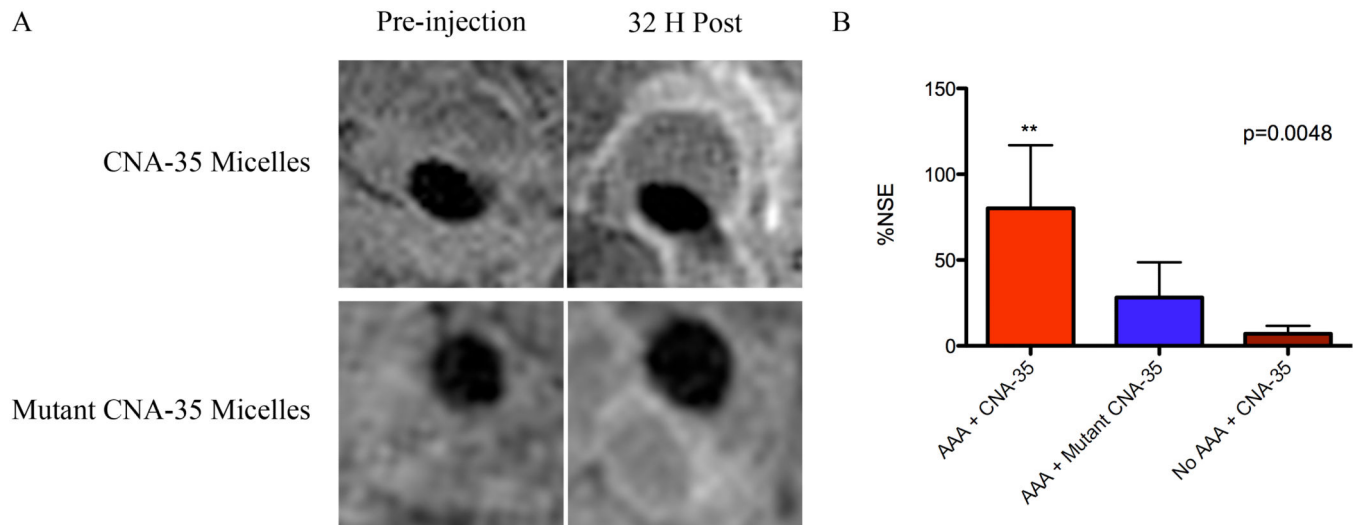
Figure 2. In vivo MR molecular imaging of collagen

(**A**) Representative images of animals bearing AAAs and injected with CNA-35 micelles or mutant CNA-35 micelles. The injection of CNA-35 micelles caused an important signal enhancement in the aneurysmal wall compared to mutant CNA-35 micelles. The Normalized Signal Enhancement percentage deriving from the aneurysmal wall was calculated in both groups and is plotted in (**B**) The data analysis is presented as mean ± standard deviation. CNA-35 micelles injected in animals with abdominal aortic aneurysms caused a significant MR signal enhancement compared to mutant CNA-35 micelles and CNA-35 micelles injected in healthy animals, ** $p < 0.01$
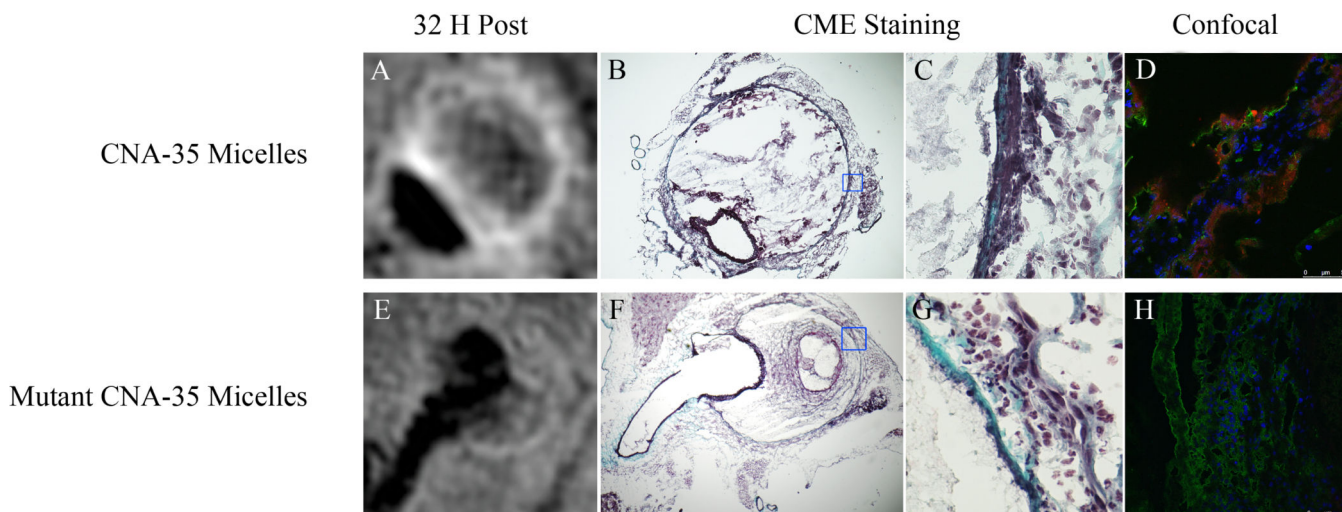
32 H Post · CME Staining · Confocal

Figure 3. Correlation of in vivo MRI findings with histological sections and confocal fluorescence microscopy

(A) Typical image of an aneurysm after the injection of CNA-35 micelles showing MR signal enhancement in the aneurysmal wall. **(B)** Corresponding histological section stained with Combined Masson Elastin (CME) showing the presence of collagen in the areas of signal enhancement. **(C)** Represents a 40× magnification of the remodeled adventitia with collagen stained in blue. **(D)** Representative image of fluorescent confocal microscopy showing the precise colocalization of CNA-35 micelles (red) with Collagen-I staining (green). **(E)** Typical image of an aneurysm after the injection of mutant CNA-35 micelles showing no significant MR signal enhancement in the aneurysmal wall. **(F)** Corresponding histological section confirming the presence of collagen stained in blue on the 40× magnification shown in **(G)**. **(H)** Representative image of fluorescent confocal microscopy of animals injected with mutant CNA-35 micelles showing no micelles in the areas of collagen staining (green).
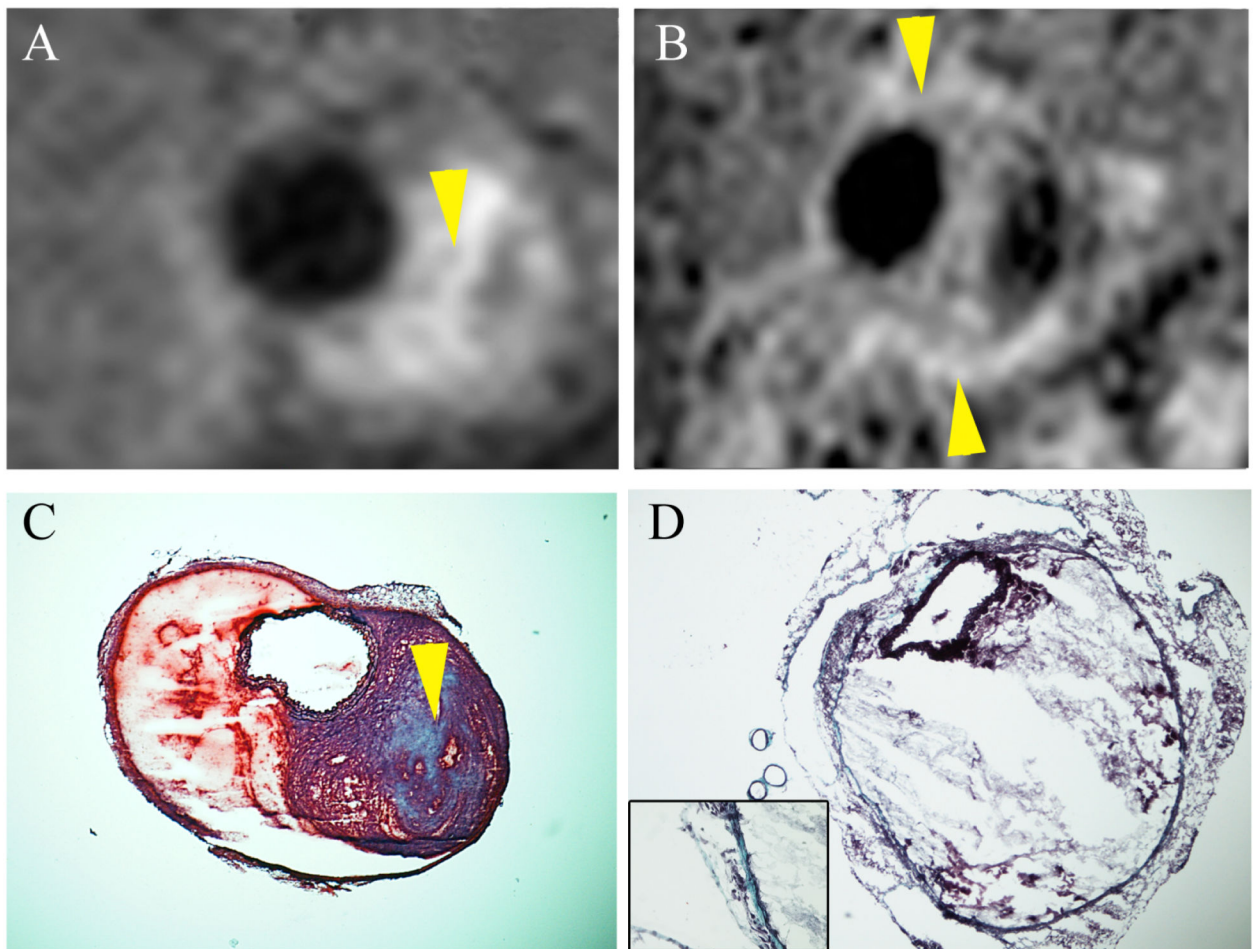
Figure 4. Spatial correlation between the pattern of MR signal enhancement and the collagen content observed by histology

(A) Representative image of a collagen-rich aneurysmal lesion after the injection of CNA-35 micelles. The high collagen content was confirmed to be present in the area of MR signal enhancement (arrows) by Combined Masson Elastin (CME) histological staining as shown in (C). (B) Representative image of a collagen-poor aneurysmal lesion after the injection of CNA-35 micelles. A thin layer of collagen was identified by CME staining in the region of MR signal enhancement (arrows) as shown in (D).
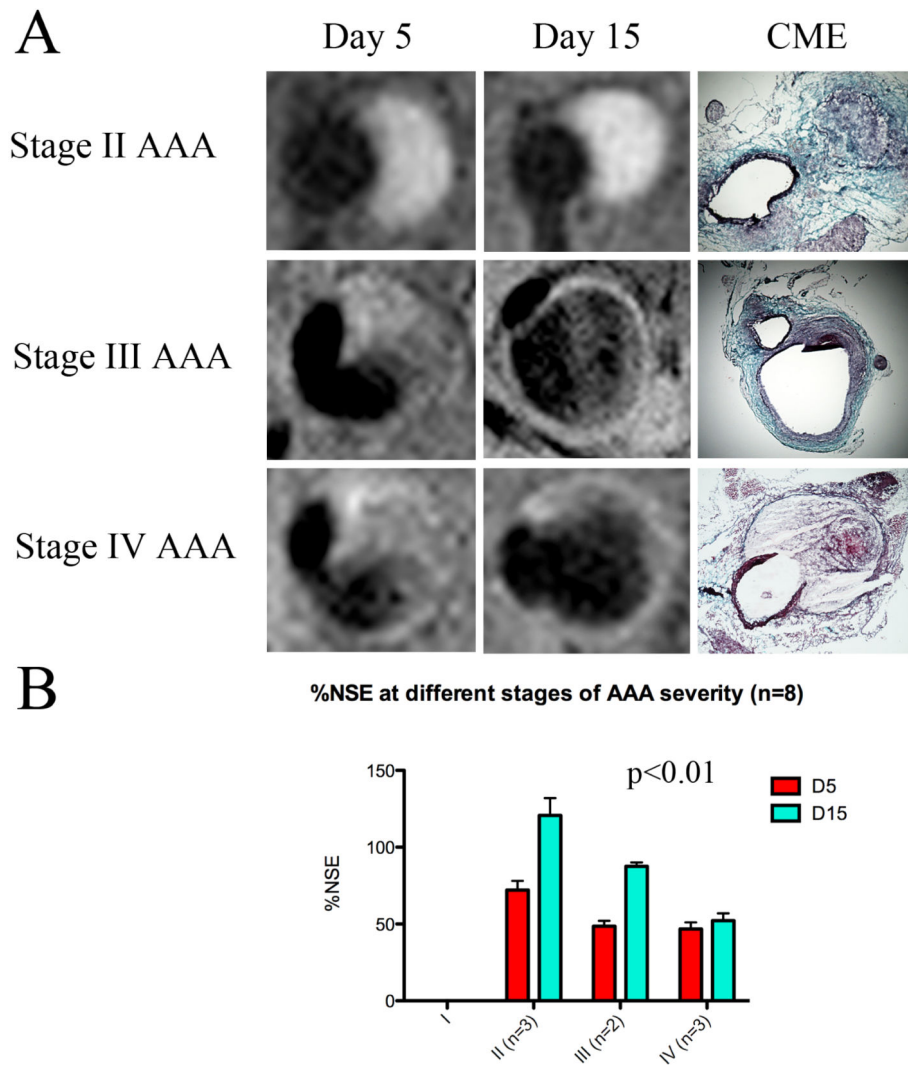
Figure 5. CNA-35 enhanced MR imaging of abdominal aortic aneurysms of increasing severity at early and late stage of development and complications

(A) Typical images of stage II, III and IV aneurysms obtained after CNA-35 injection at day 5 and day 15 of AAA development. Corresponding histological sections stained with Combined Masson Elastin (CME) are shown in the third column. **(B)** Quantification of aneurysm severity – increasing from stage I to IV - and normalized signal enhancement percentage (%NSE) relative to CNA-35 injection in a group of mice (n=8).